

*Naturalistic arm movements during
obstacle avoidance in 3D and the
identification of movement primitives*

**Britta Grimme, John Lipinski & Gregor
Schöner**

Experimental Brain Research

ISSN 0014-4819

Volume 222

Number 3

Exp Brain Res (2012) 222:185-200

DOI 10.1007/s00221-012-3205-6



 Springer

Your article is protected by copyright and all rights are held exclusively by Springer-Verlag. This e-offprint is for personal use only and shall not be self-archived in electronic repositories. If you wish to self-archive your work, please use the accepted author's version for posting to your own website or your institution's repository. You may further deposit the accepted author's version on a funder's repository at a funder's request, provided it is not made publicly available until 12 months after publication.

Naturalistic arm movements during obstacle avoidance in 3D and the identification of movement primitives

Britta Grimme · John Lipinski · Gregor Schöner

Received: 8 September 2011 / Accepted: 24 July 2012 / Published online: 23 August 2012
© Springer-Verlag 2012

Abstract By studying human movement in the laboratory, a number of regularities and invariants such as planarity and the principle of isochrony have been discovered. The theoretical idea has gained traction that movement may be generated from a limited set of movement primitives that would encode these invariants. In this study, we ask if invariants and movement primitives capture naturalistic human movement. Participants moved objects to target locations while avoiding obstacles using unconstrained arm movements in three dimensions. Two experiments manipulated the spatial layout of targets, obstacles, and the locations in the transport movement where an obstacle was encountered. We found that all movement trajectories were planar, with the inclination of the movement plane reflecting the obstacle constraint. The timing of the movement was consistent with both global isochrony (same movement time for variable path lengths) and local isochrony (same movement time for two components of the obstacle avoidance movement). The identified movement primitives of transport (movement from start to target position) and lift (movement perpendicular to transport within the movement plane) varied independently with obstacle conditions. Their scaling accounted for the observed double peak structure of movement speed. Overall, the observed naturalistic movement was astoundingly

regular. Its decomposition into primitives suggests simple mechanisms for movement generation.

Keywords Motor control · 3D human arm movements · Obstacle avoidance · Movement primitives · Path selection

Introduction

Everyday human arm movements such as reaching for objects and transporting them from one place to another often entail obstacle avoidance. When reaching for the milk on the coffee table, for instance, we may need to avoid crashing into cups, plates, or the cake. How the central nervous system (CNS) generates such smooth and well-controlled trajectories is not yet fully understood.

One long-standing approach in movement science has been to search for regularities and invariances in movement trajectories. This has led to the discovery of the piecewise planarity of end-effector paths (Soechting and Terzuolo 1987), the 2/3 power law (Lacquaniti et al. 1983) that relates the curvature of the end-effector path to the speed of end-effector, the isochrony principle (Viviani and McCollum 1983) that predicts a roughly constant movement duration independent of the distance traveled, bell-shaped velocity profiles for straight hand paths (Morasso 1981), and valleys in the speed profile in regions of high curvature (Abend et al. 1982). Typically, the invariances are only approximate and are not observed under all conditions (Sternad and Schaal 1999). Theoretical accounts for observed regularities and invariances have invoked principles of optimality such as maximizing smoothness (Flash and Hogan 1985; Uno et al. 1989), minimizing variance of final end-effector position (Harris and Wolpert 1998), or minimizing effort (Hasan 1986).

B. Grimme (✉) · J. Lipinski · G. Schöner
Institut für Neuroinformatik, Ruhr University Bochum,
Bochum, Germany
e-mail: britta.grimme@ini.rub.de;
britta.grimme@ruhr-uni-bochum.de

J. Lipinski
e-mail: 2johnlipinski@gmail.com

G. Schöner
e-mail: gregor.schoener@ini.ruhr-uni-bochum.de

Most of this experimental and theoretical work has been based on restricted movement conditions. Do the optimality principles and invariants extend to complex daily life movements? Few studies have directly looked at naturalistic 3D movements in which objects are transported relative to a surface. Arm movement studies in 3D have included aimless movements of the arm (scribbles) (Morasso 1983; Pollick et al. 2009; Viviani et al. 2009), drawing movements of 3D figures (Soechting and Terzuolo 1987; Maoz et al. 2009), ellipses (Sternad and Schaal 1999), figure eights (Soechting and Terzuolo 1987; Pellizzer et al. 1992), or point-to-point movements (Atkeson and Hollerbach 1985). Surprisingly, most movement studies that included obstacle avoidance were merely performed in 2D (Abend et al. 1982; Flash and Hogan 1985; Dean and Brüwer 1994; Sabes and Jordan 1997; Saling et al. 1998). The few recent relevant 3D studies either consider arm movements in monkeys (Torres and Andersen 2006) or focus on the influence of non-target objects that are not placed in the line of reaching (Chapman and Goodale 2008).

The question, if invariance and principles of optimality apply to complex, naturalistic movement has become theoretically important in light of the proposal that such movements may be built from a number of movement primitives. The idea might go back to the observation that spinal neurons generate convergent force-fields at the end-effector (Bizzi et al. 1991), but has gained traction when it was linked to principles of learning (Schaal and Schweighofer 2005). In this conception, a complex movement trajectory is thought of as built from pieces of trajectory or, equivalently, of vector-fields that are linearly combined. When conceived as a problem of imitation learning, the weights for linear combination may be determined to approximate demonstrated trajectories (Ijspeert et al. 2001).

The precise definition of movement primitives is still somewhat in flux (see Degallier et al. (2011) for a recent review). Here, we propose that movement primitives should be invariants. Specifically, we propose that complex movements can be decomposed into components that have the regularity properties observed for simple movements and are invariant under some, if not all task conditions. If primitives depend on task conditions, then this dependence should take the form of simple scaling laws.

In the experiments reported here, participants held an object in their hand, which they moved toward target locations while avoiding obstacles in 3D. Our analysis probes the extent to which such naturalistic end-effector movements in 3D exhibit the same kinds of regularities and invariances observed in more restricted movements. Moreover, we seek to identify a parsimonious decomposition of such trajectories into movement primitives that explain the invariants.

We find that naturalistic 3D end-effector movements are largely planar and can be decomposed into a lift/descend and a transport component, whose simultaneous execution accounts for target acquisition and obstacle avoidance. We examine how these components adjust to the spatial configuration of obstacle and target, in part, independently of each other. We use this decomposition to explain seemingly complex observed features of the kinematics such as a double peak in end-effector velocity during obstacle avoidance. Moreover, the decomposition into movement primitives leads to a natural extension of the principle of local isochrony.

The article is organized as follows: The “**Methods**” section reviews experimental and analysis methods of the two studies performed. The first experiment probes the dependence of obstacle avoidance on the spatial layout of obstacles relative to movement targets. The second experiment looks specifically at how the position of an obstacle early versus late in a transport movement affects movement timing. In the “**Results**” section, we describe the characteristics of naturalistic 3D obstacle avoidance movements with a special focus on the identification of movement primitives. Specifically, we derive a lift and a transport primitive from the planarity invariant of naturalistic 3D movements and use these to investigate the isochrony principle, the time structure of end-effector velocity, as well as the end-effector spatial path. Finally, in the “**General discussion**”, we review our findings and highlight conceptual and theoretical implications.

Methods

Participants

Fifteen healthy, right-handed (determined by self-report) participants took part in this study. Each one gave written informed consent after a detailed explanation of the task.

Experiment 1

Experimental setup

Ten participants (6 male, 4 female, 26.5 ± 0.76 (SE) years) performed a simple obstacle avoidance task on a table by relocating a cylindrical object from a starting position to one of two possible target positions which differed in distance and direction, see Fig. 1a.

Participants were seated in a height adjustable, rigid chair in front of a table. The height of their shoulder was adjusted to 110 cm. To prevent participants from moving their body trunk, we fixed the trunk with seatbelts. At the beginning of each trial, the right forearm rested at a lateral

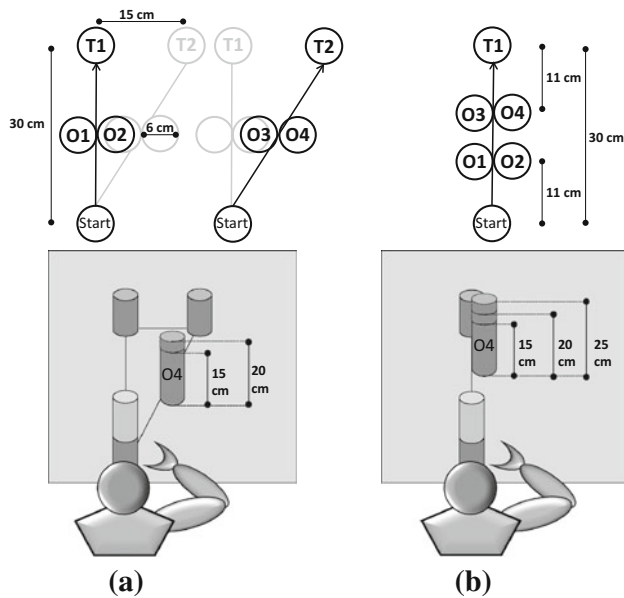


Fig. 1 Experimental setup. **a** Experiment 1. Target 1 (T1) was located in *straight* ahead direction and target 2 (T2) was additionally shifted 15 cm to the *right* and thus positioned in a direction diagonal to the starting position. Obstacles were located at mid-distance between start and target either to the *left* or rather to the right of the *straight line* connecting start and target. Obstacle locations O1 and O2 were only applied in combination with T1, whereas obstacle locations O3 and O4 were combined with T2. Obstacles were of two different heights. **b** All movements headed for T1. Obstacles were located nearby the starting position (O1 and O2) or nearby the target location (O3 and O4) and were of three different heights

support surface on the table, whereas the left arm gripped a wooden cylinder on the left side of the workspace to stabilize the body posture. After hearing an auditory signal, the participants were instructed to reach for a cylindric object located directly in front of them on top of the starting platform (6 cm in diameter, 10 cm in height) at a distance of 9 cm from the front edge of the table. The object consisted of a small wooden part (2.5 cm in height) which enables stable positioning and a top portion made out of Styrofoam (10 cm in height). Participants were instructed to transport the object to one of two possible target platforms:

1. Target 1 (6 cm in diameter, 10 cm in height): At a distance of 30 cm away from the starting platform in straight ahead direction.
2. Target 2 (6 cm in diameter, 10 cm in height): Additionally shifted 15 cm to the right, thus positioned in a direction diagonal to the starting position.

During movement participants had to avoid an obstacle (6 cm in diameter, 15 cm (small) or 20 cm (medium) in height) which was positioned at mid-distance between start and target directly to the left or rather to the right of the straight line connecting start and target. In each condition,

there was only one obstacle present which did not block the view toward the target. The end of the data collection was indicated by an auditory signal which differed from the starting signal.

The actual recording session was preceded by few warm-up trials to familiarize the participants with the task. No instruction was given about how to avoid the obstacle (e.g. passing over the obstacle or sideways around the obstacle). Nor were accuracy constraints placed on the movements. Participants were discouraged from making corrective actions after the movement ended. They were told to perform the movement with a natural and consistent speed. Trials in which participants collided with the obstacle during avoidance movement were discarded and rerun. Altogether, participants performed 10 experimental conditions: 2 obstacle heights, 2 obstacle positions, 2 target positions and for each target one condition without obstacle ($2 \times 2 \times 2 + 2$). Participants completed 15 repetitions of each of the 10 configurations for a total of 150 pseudo-randomly ordered trials. Symbols which are used for describing the 10 configurations are composed out of target position, obstacle position, and obstacle height, see Table 1. Obstacle positions are also depicted in Fig. 1a. For statistical analysis and computation of mean data, we discarded the first three trials of each condition because they deviated most in terms of movement time and spatial paths.

Experiment 2

Experimental setup

Five healthy, right-handed participants (3 male and 2 female, 27.6 ± 0.81 (SE) years) contributed to this experiment. The experimental setup was similar to the previous experiment with the following modifications:

- Participants had to perform their movements to only one target in straight ahead direction (target 1 of the previous experiment).
- Obstacles were of three different heights: 15 cm (small), 20 cm (medium), and 25 cm (tall).
- Obstacles were shifted from mid-distance nearer to the start- (11 cm from start) or to the target-cylinder (11 cm from target and respectively 19 cm from start). Thus, obstacles were located at 4 positions (2 distances (near, far) \times 2 directions (left, right)).

Accordingly, participants performed a total of 13 experimental conditions: 3 obstacle heights, 2 obstacle directions (left, right), and 2 obstacle distances (near, far) + one condition without obstacle ($3 \times 2 \times 2 + 1$). Participants completed 12 repetitions of each of the 13 configurations for a total of 156 pseudo-randomly ordered

Table 1 Symbols describing target and obstacle properties for experiment 1

Target position		Obstacle position			Obstacle height	
Straight	Diagonal	No obstacle	Left	Right	Small: 15 cm	Medium: 20 cm
T1	T2	–	O1, O3	O2, O4	S	M

Symbols are composed as triple out of target position, obstacle position, and obstacle height. For example, T1O1S denotes a small obstacle on the left position of the straight line which connects start and target 1. Note that O1 and O2 are only applied when the movement aims for target 1, while O3 and O4 are only combined with target 2

trials. Symbols which are used for describing the 13 configurations are composed out of obstacle position and obstacle height, see Table 2. Obstacle positions are also depicted in Fig. 1b. For statistical analysis and computation of mean data, we discarded the first two trials of each condition because they deviated most in terms of movement time and spatial paths.

Data collection and processing

Movements were recorded with the Visualeyex (Phoenix Inc.) motion capture system VZ 4000. Two trackers—each equipped with three cameras—were mounted on the wall 1.5 m above the working surface, so that both systems had an excellent view of the table (from above, from ahead, and from the right). A wireless infrared light-emitting diode (IRED) was attached to the object. The trajectories of markers were recorded in three Cartesian dimensions at a sampling rate of 110 Hz based on a reference frame anchored on the table. The starting position projected to the table was taken as the origin of each trajectory, i. e. (0,0,0) in 3D Cartesian space; x = horizontal, y = depth, z = vertical. All data points were filtered by using a second-order zero-phase forward and reverse Butterworth filter (Matlab “butter” and “filtfilt” function) with cutoff frequency at 5.5 Hz. After filtering, movement onset was estimated (from the object-IRED) as the first point in time where acceleration drops under 15 % of maximum acceleration, determined backwards in direction of movement beginning, starting from the moment of maximum acceleration. Termination of movement was estimated with respect to tangential velocity and distance to the start platform. The time series of tangential velocity $s(t)$ and torsion $T(t)$ were estimated using the vector formulae:

$$s(t) = \|\dot{\mathbf{x}}(t)\| \tag{1}$$

$$T(t) = \frac{(\mathbf{v}(t) \times \mathbf{a}(t)) \cdot \mathbf{j}(t)}{\|\mathbf{v}(t) \times \mathbf{a}(t)\|^2} \tag{2}$$

where $\mathbf{v}(t) = \dot{\mathbf{x}}(t)$ is the velocity vector, $\mathbf{a}(t) = \ddot{\mathbf{x}}(t)$ is the acceleration vector, and $\mathbf{j}(t) = \dot{\mathbf{x}}(t)$ is the jerk vector with $\mathbf{x}(t) = [x(t), y(t), z(t)]^T$ being the 3D end-effector movement trajectory.

Amount of path change induced by obstacle avoidance

As a measure of changes in spatial path induced by obstacle avoidance Δ , we computed the sum of euclidean norms of the differences between mean obstacle-trajectories and the corresponding mean no-obstacle trajectory for each obstacle condition and each participant. Therefore, we re-sampled trajectories to consist of 100 data points. Using the Matlab function “interp1”, we performed a linear interpolation of the trajectory values to obtain data points for 1–100 % of movement time.

$$\Delta_{(\text{tar,obs})} = \sum_{t=1}^{100} \|\mathbf{x}_{(\text{tar,obs})}(t) - \mathbf{x}_{(\text{tar,-})}(t)\| \tag{3}$$

where ‘tar’ denotes the target condition (tar = 1,2 for experiment 1), ‘obs’ the obstacle condition, and ‘–’ no obstacle.

Plane of motion

As a means to describe the chosen plane of motion during obstacle avoidance, we computed the elevation angle $\phi(t)$ between the plane of motion and the horizontal plane described by the table. First, we computed the unit

Table 2 Symbols describing obstacle properties for experiment 2

Obstacle position					Obstacle height		
No obstacle	Left, near	Right, near	Left, far	Right, far	Small: 15 cm	Medium: 20 cm	Tall: 25 cm
–	O1	O2	O3	O4	S	M	T

Symbols are composed out of obstacle position and obstacle height. For example, O1S denotes a small obstacle located nearby the start position on the left of the straight line which connects start and target

binormal vector $\mathbf{B}(t)$ of the 3D end-effector trajectory based on a reference frame that is anchored on the table and centered on the marker on top of the moved object in its initial position.

$$\mathbf{B}(t) = \mathbf{T}(t) \times \mathbf{N}(t) \tag{4}$$

where $\mathbf{T} = \frac{\dot{\mathbf{x}}(t)}{\|\dot{\mathbf{x}}(t)\|}$ is the unit tangent vector and $\mathbf{N} = \frac{\dot{\mathbf{T}}(t)}{\|\dot{\mathbf{T}}(t)\|}$ is the unit normal vector. Then, we transformed Cartesian coordinates of $\mathbf{B}(t)$ into spherical coordinates using the Matlab function “cart2sph” and thereby obtained the angle $\beta(t)$ which is enclosed by the unit binormal vector $\mathbf{B}(t)$ and the table plane. The elevation angle of the movement plane was then determined as

$$\phi(t) = 90^\circ - \beta(t) \tag{5}$$

Finally, the mean elevation angle ϕ was computed as a circular mean over 30–60 % of movement time when torsion was minimal.

Decomposition of the end-effector path into the transport primitive and the lift/descend primitive

We decompose the end-effector path into two primitives: the transport component and the lift/descend component. The transport component, τ , is obtained by projecting the path onto the straight line connecting the start position to the target position. By choice of coordinate system, this corresponds to the Euclidean y-component (for target 2 in experiment 1 after a rotation of the coordinate frame). The lift/descend component,

$$\ell(t) = \sqrt{x(t)^2 + z(t)^2} \tag{6}$$

is the orthogonal complement. Here, we shifted the z-axis up such that the marker on the transported object was at the origin prior to movement onset. Note that the lift component is defined to only be positive. This is consistent with our experimental setting where start and target positions are at the same height. Because the movement is approximately planar, these components largely reflect the movement within the movement plane as illustrated in Fig. 2. The tangential velocity,

$$s(t) = \sqrt{\dot{\ell}(t)^2 + \dot{\tau}(t)^2}, \tag{7}$$

is thus composed of the velocities of the two primitives.

Statistical analysis

Single means for each participant for each condition were calculated and entered into a repeated measures analysis of variance (ANOVA) with three main factors in SPSS. For

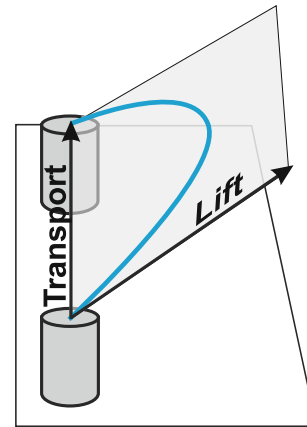


Fig. 2 Decomposition of the end-effector path into the lift/descend primitive and the transport primitive

experiment 1, main factors were obstacle position (left, right), obstacle height (small, medium), and target position (target 1, target 2). For experiment 2, we used obstacle position (left, right), obstacle distance (near, far), and obstacle height (small, medium, tall) as main factors. Where appropriate, F statistics were corrected for violations of the sphericity assumption using the Greenhouse-Geisser correction. Pair-wise comparisons were performed using Student’s *t* tests, the *P* values were adjusted for multiple comparisons using Bonferroni correction. Data values are reported as mean ± standard error (SE). Alpha was set at *P* = 0.05 for all statistical analyses.

Results

Results: Experiment 1

Spatial paths

All spatial end-effector paths reflect obstacle avoidance and differ with respect to target and obstacle positions, see Fig. 3. The amount of path change induced by obstacle avoidance (Eq. (3)) is significantly higher for obstacles on the right compared to obstacles on the left ($F_{(1,9)} = 28.938, P < 0.001$) as well as for medium obstacles compared to small obstacles ($F_{(1,9)} = 205.424, P < 0.001$). Further, there is a highly significant obstacle position × obstacle height interaction ($F_{(1,9)} = 44330.605, P < 0.001$) revealing a stronger increase in the amount of path change with obstacle height if the obstacle is positioned on the right. This is consistent with the observation that obstacles on the left were avoided with a stronger sideway strategy (see below).

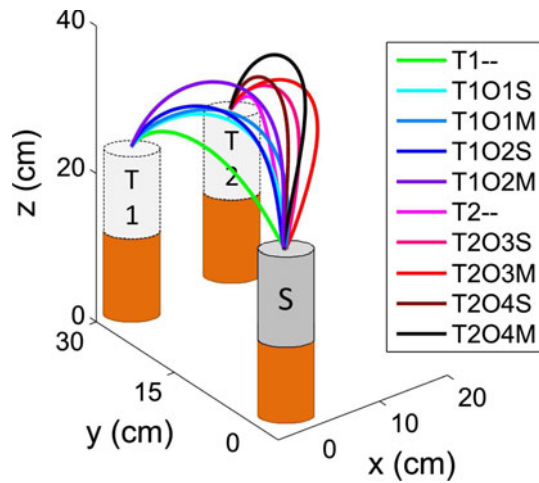


Fig. 3 Mean (over all participants) 3D obstacle avoidance paths from the starting position (S) to both target positions (T1 and T2)

Planarity and obstacle avoidance strategy

Although virtually unrestricted in space, obstacle avoidance paths are approximately planar (Fig. 4a). This is indicated by low levels of torsion during the movement, see Fig. 4b. Absolute torsion averaged across obstacle conditions and participants in the middle part of movement (30–60 % of movement time) is $0.051 \pm 0.013 \text{ cm}^{-1}$. Early and late values of torsion can only be estimated unreliably as flagged by the strong variance visible in Fig. 4b.

The plane of movement illustrated in Fig. 5 reflects obstacle and target properties. The plane of motion assessed by elevation (Eq. (5)) varies significantly with obstacle position ($F_{(1,9)} = 23.47, P = 0.001$). The mean elevation angle is $57.69^\circ \pm 3.80^\circ$ for obstacles on the left and

$76.82^\circ \pm 2.12^\circ$ for obstacles on the right reflecting that obstacles on the right are more likely avoided over the top, whereas obstacles on the left are more likely avoided sideways, see Fig. 6. Similarly, the mean elevation angle ϕ is significantly smaller ($F_{(1,9)} = 23.56, P = 0.001$) for medium obstacles ($63.82^\circ \pm 3.04^\circ$) than for small obstacles ($70.69^\circ \pm 2.45^\circ$). The significant interaction between obstacle position and obstacle height ($F_{(1,9)} = 6.75, P = 0.029$) reveals that the elevation angle of the plane decreases to a greater extent with obstacle height, if the obstacle is positioned on the left.

Single trial movements from all participants show that in some conditions (e.g. T1O2M: forward target, medium obstacle on the right), variability is high as participants variably use sideways, over the top, or even mixed paths, see Figs. 5 and 6. Further, participants tend to have consistent avoidance strategies (e.g. the violet participant's trajectory is usually biased to the left, while the pink participant commonly follows the rightmost trajectories in the setup).

Double peak structure of velocity

The tangential velocity is bell-shaped in no-obstacle conditions. Near the obstacle, we often find a decrease in speed resulting in a double peak structure of velocity as shown in Fig. 7. The bimodal structure of velocity can be understood by decomposing the tangential velocity into the velocities of the transport component, $\dot{\tau}(t)$, and the lift/descend component, $\dot{\ell}(t)$. Figure 7 visualizes this decomposition by plotting the squares of these components of velocity jointly with the squared tangential velocity (Eq. (7)). Generally, the transport component of velocity is bell-shaped, whereas the lift component is bimodal as velocity is reversed and

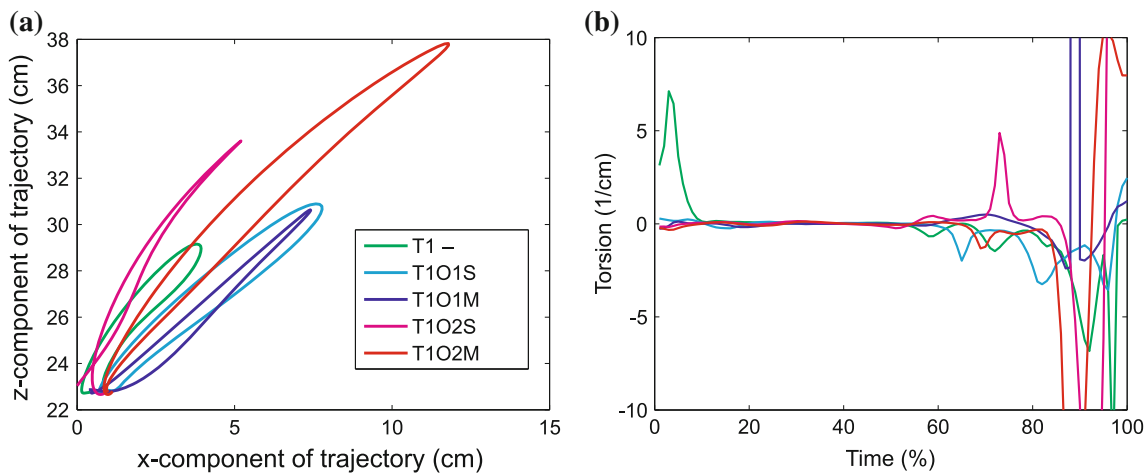


Fig. 4 Spatial paths in the coronal plane (a) and corresponding single trial torsion (b) for all obstacle conditions to target 1 of a representative participant. As torsion values are small, end-effector

paths are planar and describe different movement planes which are chosen right at movement onset according to obstacle properties

Fig. 5 Planes of movement. Single trial movement planes from each participant and each obstacle condition are shown. Colors indicate different participants (color figure online)

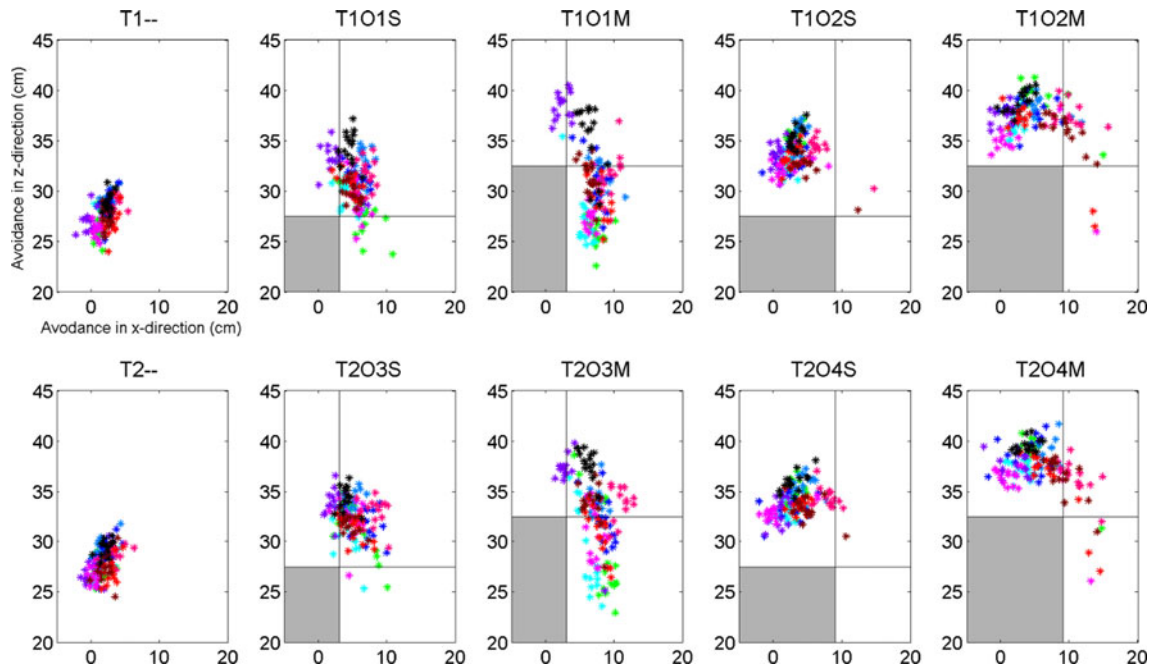
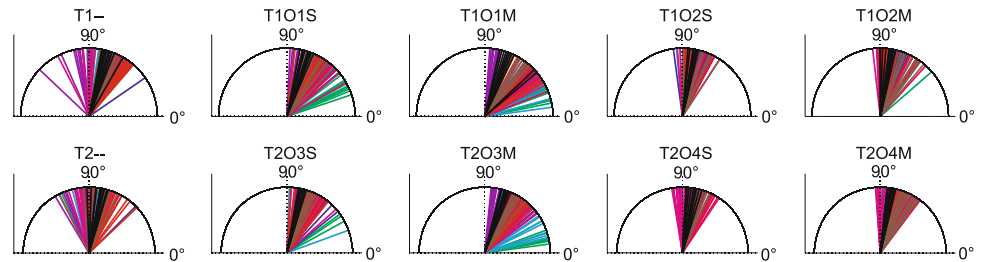


Fig. 6 Obstacle avoidance. Each point represents one movement and illustrates the avoidance in *x*-direction and *z*-direction at the time of obstacle passage. All movements from each participant are depicted. The obstacle is marked in gray. The horizontal line denotes obstacle height. Thus, all points above this line represent avoidance movements

passing over the top of the obstacle. Likewise, the vertical line denotes collision free sideways passage of the obstacle. All points on the right of this line indicate movements sideways around the obstacle and those in the upper right denote a merged avoidance strategy. Colors indicate different participants (color figure online)

goes through zero during the transition from lift to descend. In the no-obstacle condition (left), the lift component is too small for generating a double peak. The resulting bell shape comes from the transport component. A medium obstacle on the left (center, condition T2O3M) induces two peaks in the lift component with a stronger peak in the transport component leading to a single humped tangential velocity. A medium obstacle on the right (right, condition T2O4M) leads to a double peak in tangential velocity that comes from the much larger peaks in the lift/descent component.

Movement time, path length, and the isochrony principle

Movement time is independent of target conditions ($F_{(1,9)} = 0.08, P = 0.784$) but increases significantly for obstacles on the right ($F_{(1,9)} = 15.67, P = 0.003$) and with obstacle height ($F_{(1,9)} = 113.10, P < 0.001$). A significant

interaction between obstacle position and obstacle height ($F_{(1,9)} = 32.33, P < 0.001$) reveals that movement time increases to a greater extent with obstacle height, if the obstacle is positioned on the right part of the workspace (Fig. 8a). This makes sense as obstacles on the left are often avoided sideways, and thus, the obstacle's height has less impact on the avoidance movement and its duration. Similarly, path length strongly depends on obstacle and target conditions. Path length is significantly increased for the second (more distant) target ($F_{(1,9)} = 117.16, P < 0.001$), for obstacles on the right ($F_{(1,9)} = 32.36, P < 0.001$), and for medium obstacles ($F_{(1,9)} = 94.35, P < 0.001$, Fig. 8b).

Average velocity is larger for the distant target ($F_{(1,9)} = 126.70, P < 0.001$). It ranges from 43.64 ± 1.69 cm/s (mean value for all paths to target 1 \pm SE) to 48.02 ± 1.98 cm/s (mean value for all paths to target 2 \pm SE). This matches the observation that path length but not movement

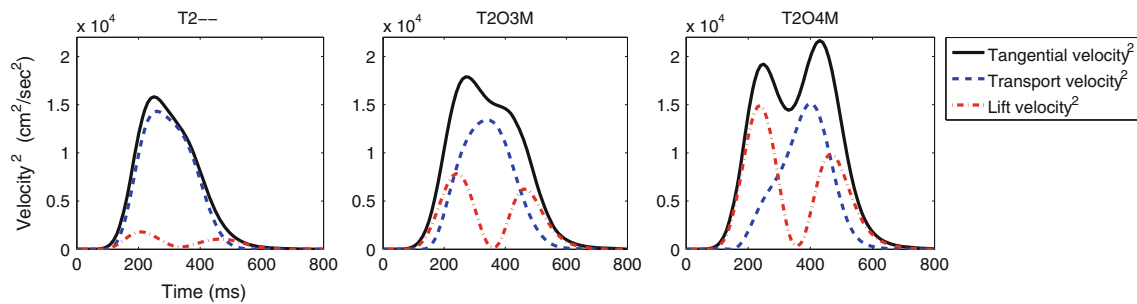


Fig. 7 Double peak structure of velocity (mean data of a representative participant). Adding the squared lift component of velocity and the squared transport component of velocity yields the squared tangential velocity, see Eq. (7)

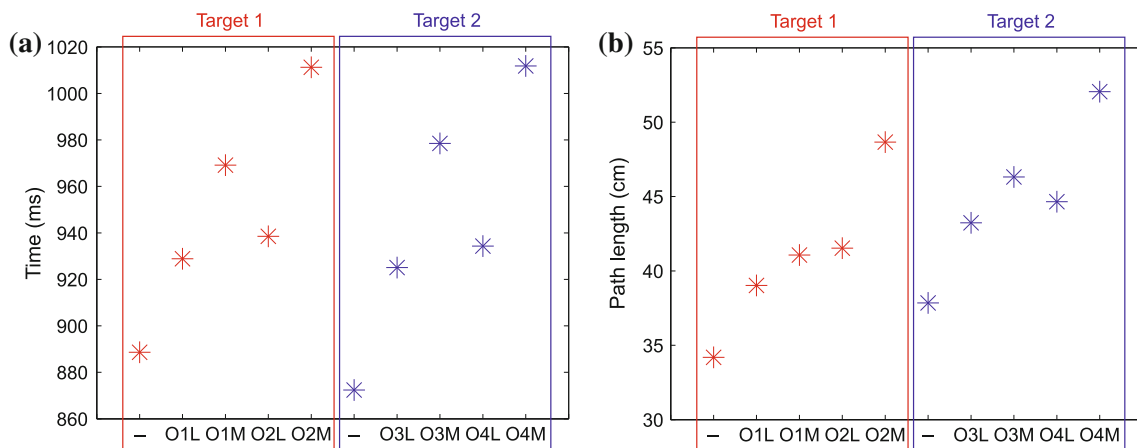


Fig. 8 Isochrony principle. Path length (b), but not movement time (a) is increased for target 2. This is consistent with the isochrony principle that predicts a constant movement duration when movement distance varies

time is larger for target 2 (isochrony, Fig. 8). More precisely, we found that both components of velocity, transport ($F_{(1,9)} = 289.85, P < 0.001$) and lift ($F_{(1,9)} = 28.98, P < 0.001$), are significantly increased for target 2. Average transport velocity ranges from 31.64 ± 0.92 cm/s (mean value for all paths to target 1 \pm SE) to 35.52 ± 1.11 cm/s (mean value for all paths to target 2 \pm SE) and average lift velocity ranges from 23.21 ± 1.25 cm/s (mean value for all paths to target 1 \pm SE) to 25.15 ± 1.36 cm/s (mean value for all paths to target 2 \pm SE).

Results: Experiment 2

The second experiment manipulates the point during the transport movement at which the obstacle is encountered so that the time structure of the induced obstacle avoidance movement and the coordination between the two primitives are probed.

Spatial paths

The amount of path change induced by obstacle avoidance is significantly increased for obstacles on the right

compared to obstacles on the left ($F_{(1,4)} = 71.008, P = 0.001$) as well as for tall obstacles compared to small obstacles ($F_{(1,027,4,108)} = 51.616, P = 0.002$). Additionally, there is a significant obstacle position \times obstacle height interaction ($F_{(2,8)} = 52.778, P < 0.001$) which reveals a stronger increase in the amount of path change with obstacle height if the obstacle is positioned on the right. There is no significant effect of obstacle distance on the amount of path change ($F_{(1,4)} = 1.900, P = 0.240$).

The contrast between obstacle avoidance early versus late in the movement can be best visualized by decomposing the trajectory into the transport primitive and the lift/descend primitive as shown in Fig. 9a. Whereas the lift component is very similar for near and far obstacles, the transport component varies substantially, being delayed for obstacles early in the movement path. At 30, 50, and 70 % of movement time, we did not find any significant differences in lift excursion between near and far obstacles (30 %: $F_{(1,4)} = 0.220, P = 0.664$, 50 %: $F_{(1,4)} = 1.3322, P = 0.313$, 70 %: $F_{(1,4)} = 4, 65, P = 0.098$) while the transport component was significantly modulated by obstacle distance (30 %: $F_{(1,4)} = 86.66, P = 0.001$, 50 %: $F_{(1,4)} = 239.12, P < 0.001$, 70 %: $F_{(1,4)} = 87.47, P = 0.001$).

Plotting the lift against the transport component in Fig. 9b reveals how the spatial path is skewed differently depending on obstacle conditions. The path rises steeply in the early movement phase for near obstacles and falls steeply in the end phase for far obstacles. Interestingly, the lift components in Fig. 9a are bell-shaped when plotted against time but skewed when plotted as paths against the transport component, see Fig. 9b.

The invariance of the lift component contrasts with the modulation of the transport component for early versus late obstacles. For a statistical analysis of the invariance of the lift shape, we evaluated the points in time at which 50 and 100 % of maximal lift excursion is reached. The point of 50 % excursion is reached twice, once for lift and once for descent. The means of these times were as follows: 50 % (upwards): 242.70 ± 3.61 ms (near obstacle) versus 240.27 ± 2.27 ms (far obstacle); 100 %: 402.10 ± 4.40 ms (near obstacle) versus 401.27 ± 3.20 ms (far obstacle); 50 % (downwards): 589.50 ± 7.92 ms (near obstacle) versus 589.40 ± 9.42 ms

(far obstacle). These times did not depend significantly on the distance of the obstacle (50 % (lift): $F_{(1,4)} = 0.832$, $P = 0.413$, 100 %: $F_{(1,4)} = 0.094$, $P = 0.775$, 50 % (descent): $F_{(1,4)} < 0.001$, $P = 0.985$). In contrast, for the transport component, the points in time to reach 25, 50, and 75 % of the transport amplitude differed significantly between the obstacle near versus far condition: (25 %: $F_{(1,4)} = 144.97$, $P < 0.001$, 50 %: $F_{(1,4)} = 362.43$, $P < 0.001$, 75 %: $F_{(1,4)} = 3054.75$, $P < 0.001$). Figure 9a illustrates that the time to reach any of the three points is larger for near obstacles.

Figure 9c and d show how both components of the trajectory are influenced by obstacle height. First, an increase of obstacle height leads to a larger amplitude of the lift component ($F_{(1,019,4,076)} = 37.544$, $P = 0.003$). The transport component is also modulated: For near obstacles, the transport trajectories diverge in an early part of movement as tall obstacles delay the transport component's progression to a greater extent than small obstacles,

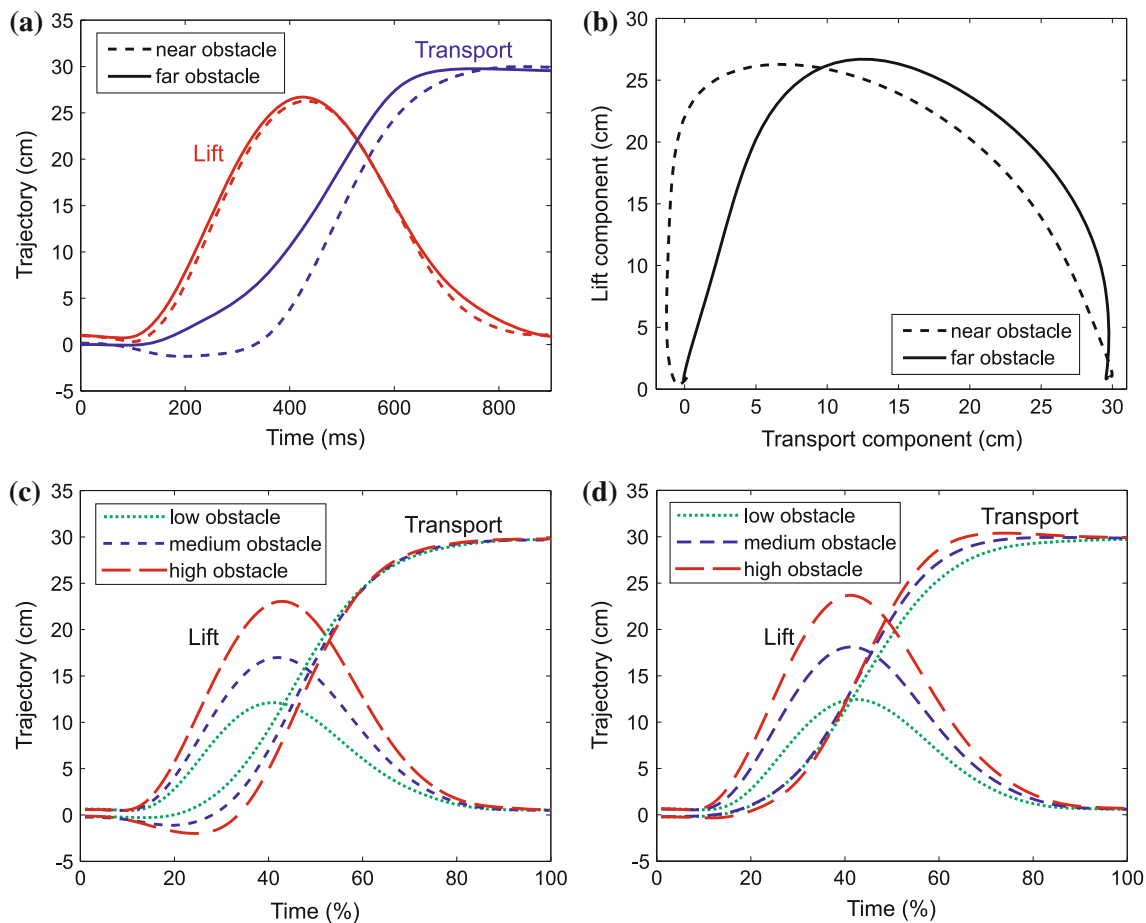


Fig. 9 a Single trial lift and transport components of trajectory for corresponding near and far obstacle conditions (O2T, O4T) of a representative participant. In b the lift component is plotted against the transport component, allowing a direct view into the movement plane. Beyond, mean (over all participants) lift and transport

components of trajectory are shown for near (c) and far (d) obstacles of varying heights. With growing height the amplitude of the lift component increases. The height of the obstacle modulates the early part of the transport component for early obstacles and correspondingly the late part of the transport component for late obstacles

even inducing a small backwards movement. At 30 % of time, the transport component is significantly smaller with increasing obstacle height ($F_{(2,8)} = 11.800$, $P = 0.004$). A significant obstacle position \times obstacle height interaction ($F_{(2,8)} = 11.101$, $P = 0.005$) reveals a stronger decrease in the transport component with obstacle height if the obstacle is positioned on the right. This loss of progression is compensated by a steeper slope in later portions of the movement. There is a corresponding divergence of transport trajectories in a late movement phase for far obstacles, see Fig. 9d. At 70 % of time, the transport component is significantly larger with increasing obstacle height ($F_{(1,025,4,104)} = 53.310$, $P = 0.002$). A significant obstacle position \times obstacle height interaction ($F_{(1,028,4,114)} = 16.568$, $P = 0.014$) reveals a stronger increase of the transport component with obstacle height if the obstacle is positioned on the right.

Planarity and obstacle avoidance strategy

We reproduced Experiment 1 by finding low levels of torsion indicating that obstacle avoidance movements are approximately planar. The selected movement plane depends on obstacle positions and heights. The elevation angle of the movement plane decreases significantly with obstacle height ($F_{(2,8)} = 26.78$, $P < 0.001$). Pairwise comparisons using the Bonferroni correction detected a significant decrease in the elevation angle when obstacle height changes from small to medium ($P = 0.005$), from small to tall ($P = 0.014$), and from medium to tall ($P = 0.041$). The mean elevation angle is $62.52^\circ \pm 4.58^\circ$ for small obstacles, $56.83^\circ \pm 4.25^\circ$ for medium obstacles, and $46.23^\circ \pm 5.03^\circ$ for tall obstacles. This is consistent with a change of avoidance strategy in which avoidance is increasingly sideways for increasing obstacle height. Similarly, the plane of motion varies significantly with obstacle position. The elevation angle is increased for obstacles on the right as the mean angle is $40.49^\circ \pm 8.04^\circ$ for obstacles on the left and $69.90^\circ \pm 3.30^\circ$ for obstacles on the right ($F_{(1,4)} = 12.02$, $P = 0.026$). This is consistent with a change of avoidance strategy in which rightward obstacles are avoided over the top. The distance from the starting position to the obstacle has no significant effect on the choice of movement plane ($F_{(1,4)} = 2.788$, $P = 0.171$).

Double peak structure of velocity

As in Experiment 1, we often observe a double peak structure in the speed profile of obstacle avoidance movements. The amplitude of the velocity peaks on either side of the velocity valley depends on the distance between the obstacle and the start platform. A repeated measures ANOVA for obstacle conditions O2M, O2T, O4M, O4T

with 4 participants¹ shows that the first peak of velocity is significantly larger for far obstacles compared to near obstacles ($F_{(1,3)} = 17.12$, $P = 0.026$). The mean peak of velocity is 103.25 ± 5.52 cm/s for far obstacles and 96.59 ± 4.57 cm/s for near obstacles. Accordingly, the second peak of velocity is smaller for far obstacles compared to near obstacles ($F_{(1,3)} = 21.60$, $P = 0.019$). The mean second peak of velocity is 104.54 ± 2.39 cm/s for far obstacles and 117.02 ± 3.56 cm/s for near obstacles. Additionally, the first ($F_{(1,3)} = 138.48$, $P = 0.001$) and second ($F_{(1,3)} = 24.26$, $P = 0.016$) peaks of velocity increase with obstacle height. The mean first peak of velocity is 93.91 ± 4.93 cm/s for medium obstacles and 106.53 ± 5.13 cm/s for tall obstacles. The mean second peak of velocity is 106.48 ± 2.44 cm/s for medium obstacles and 115.08 ± 3.22 cm/s for tall obstacles.

Again, these findings can be explained and visualized by decomposing the tangential velocity into transport and lift/descend primitives. Figure 10 shows how the squared speed emerges from the squared lift and the squared transport component of velocity in conditions with an obstacle on the right. From left to right, the height of the obstacle changes from small to tall. This increase in obstacle height comes along with a higher speed. The main effect of this development can be attributed to the lift component which is more pronounced for taller obstacles ($F_{(1,019,4,076)} = 37.544$, $P = 0.003$). In the bottom row of the figure, the obstacle is close to the starting platform, whereas the top row shows speed profiles for far obstacle conditions. The first peak of velocity is larger than the second peak for far obstacles. The order is inverted for near obstacles. This can be understood in terms of primitives: the peak of the transport velocity is pushed back in time for far versus near obstacles, so that its contribution to the tangential velocity weighs more on the first peak for far and more on the second peak for near obstacles.

Acceleration

The first peak of acceleration occurs after the same time for all obstacle conditions. There is no statistical difference in the time to reach the first acceleration peak ($F_{(11,44)} = 1.607$, $P = 0.130$). In contrast, the second peak is highly variable and occurs latest in tall-obstacle conditions, see Fig. 11a. This is especially true for obstacles positioned on the right of the workspace as obstacles on the left often do not yield a second acceleration peak. A repeated measures ANOVA for obstacle conditions on the right (O2S, O2M,

¹ One participant performed sideways avoidance movements in conditions O4T and O2T and did not show a double peak velocity structure and thus had to be discarded from this analysis. Further, conditions O2S and O4S do not show a double peak structure for most participants and were also discarded.

O2T, O4S, O4M, O4T) shows that there is a significant effect of obstacle height ($F_{(2,6)} = 89.602, P < 0.001$). Pairwise comparisons using the Bonferroni correction detected a significant increase in the time to reach the second acceleration peak when obstacle height changes from small to medium ($P = 0.021$), from small to tall ($P = 0.004$), and from medium to tall ($P = 0.008$). The mean second peak of acceleration is reached after 356.86 ± 3.86 ms for small obstacles, after 411.98 ± 4.50 ms for medium obstacles, and after 457.82 ± 5.88 ms for tall obstacles. We had observed the same synchronization of acceleration peaks in the first experiment ($F_{(8,72)} = 1.623, P = 0.133$), but report this effect here, as variation in obstacle positions along the path of the movements challenges this invariance more strongly. Shifting the obstacle nearer to the participant or further away has a major impact on the spatial path, but leaves the point in time at which the first peak of acceleration is reached unaffected ($F_{(1,4)} = 0.926, P = 0.390$).

During obstacle avoidance, the acceleration profile often shows a re-acceleration after the first peak. Looking at the lift/descent and the transport primitives of acceleration separately, we find that the first peak of lift/descent acceleration occurs at the same time for all obstacle conditions ($F_{(11,44)} = 0.855, P = 0.589$, Fig. 11b). The transport component of acceleration peaks later in time compared to the lift/descent component ($F_{(1,4)} = 14.74,$

$P = 0.018$, Fig. 11c). In the presence of obstacles, the transport component of acceleration is often bi-phasic. Its second peak largely determines the second peak of the total acceleration profile.

Time structure of obstacle passage

In order to evaluate the extent of covariation between an obstacle's position and the time structure of the induced avoidance movement, we plotted single trial velocities and marked the event of obstacle passage therein. Figure 12 shows velocity profiles of three participants for a medium height obstacle on the right in both distance conditions. This illustrates a number of observations: (1) Obstacle passage always happens after traversal of the dip in tangential velocity. Interestingly and maybe contrary to first intuition, tangential velocity is already on the rising edge during the event of obstacle passage. (2) Peaks in velocity are not strictly coupled to the event of obstacle passage. While, in the near condition, the passage happens on the rising edge of the second peak, the event of passing the obstacle is shifted to later for far obstacles. This effect is limited by the enlargement of the initial velocity peak for far obstacles (Fig. 10). (3) In contrast to obstacle passage, the point of furthest excursion from the straight path (maximum amplitude of the lift component) is strongly coupled to the speed profile. This is especially true for the

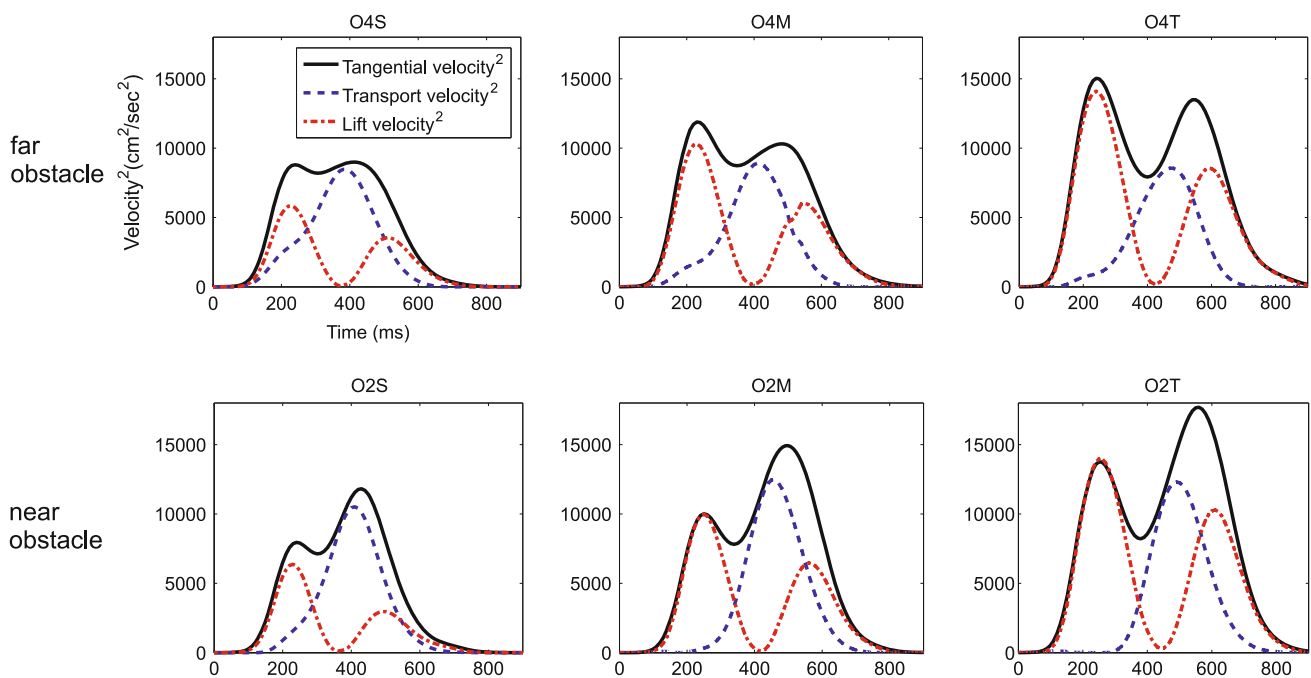


Fig. 10 Modulation of the double peak structure of tangential velocity due to varying obstacle properties. Adding the squared lift and the squared transport component of velocity yields the squared speed. From left to right obstacle height changes from small to tall. In

the bottom row speed profiles are shown for trials in which obstacles are located close to the starting position while in the top row speed profiled for far obstacle locations are depicted. Mean data from a representative participant are shown

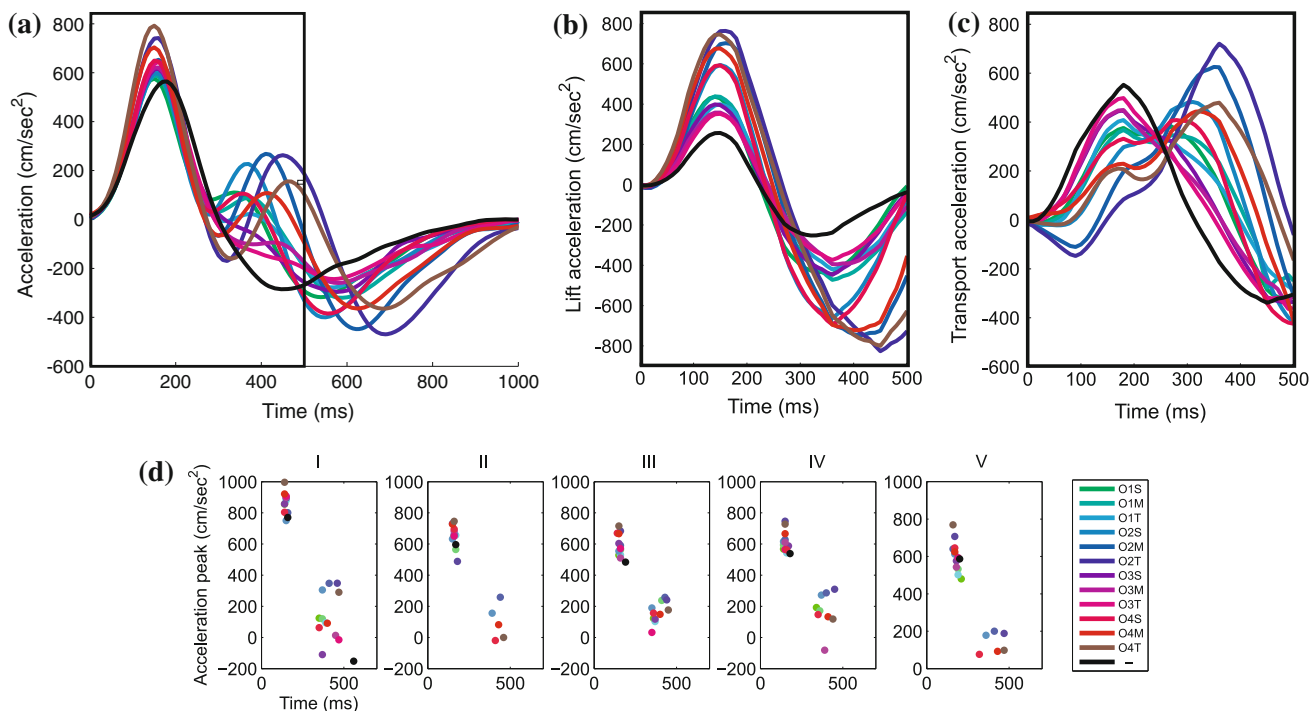


Fig. 11 Mean (over all participants) acceleration. In **a**, total acceleration and the simultaneous arriving at the first peak is shown. The *black rectangle* encloses the first 500 ms of the acceleration curve. The lift/descend (**b**) and transport (**c**) accelerations are cut off at those 500 ms. The first peak of acceleration (**a**) occurs almost simultaneously for all conditions independent of obstacle position and height. The lift (descend primitive also reaches the first peak of acceleration

at the same time for all obstacle configurations (**b**). The transport acceleration (**c**) which is often bi-phasic contributes to the first peak and provides the main part of the second peak in total acceleration. In **d** the point in time and value of the first and second acceleration peaks are shown for all participants. *Colors* indicate conditions (color figure online)

lift component, in which the point of furthest excursion coincides with the zero point in velocity. Surprisingly, the point in time with maximum excursion is roughly the same for near and far obstacles ($F_{(1,4)} = 0.049, P = 0.836$). Mean time to furthest excursion is 412.47 ± 7.89 ms for near obstacles and 411.80 ± 7.83 ms for far obstacles. This holds, although the traveled path until reaching the point of furthest excursion is significantly longer for far obstacles ($F_{(1,4)} = 22.67, P = 0.009$). Mean traveled path until furthest excursion is 22.65 ± 0.52 cm for near obstacles and 24.30 ± 0.77 cm for far obstacles. In light of the fact that the first peak of lift velocity is equal for near and far obstacles ($F_{(1,4)} = 0.64, P = 0.467$), the modulation of the transport component is solely responsible for the isochronous arrival at the point of furthest excursion for near and far obstacles. This modulation strengthens the first part of total speed until the point of furthest excursion and subsequently weakens the second part of total speed.

General discussion

In this work, we investigated naturalistic 3D obstacle avoidance movements. We analyzed the spatial path and its

decomposition into movement primitives, the planarity of movement path, the dependence of the movement plane on the obstacle configuration, the velocity structure and the isochrony principle. Some of these analyses had been performed for 2D movements, for aimless 3D movements, as well as for drawing movements of 3D figures, but not for naturalistic 3D obstacle avoidance movements, in which objects are transported relative to a surface. We also evaluated the timing and spatial structure of movements relative to obstacle conditions. This is an important aspect which goes beyond most previous work. In the following paragraphs, we summarize our findings and conclusions for the investigated aspects.

Planarity and obstacle avoidance strategy

Although unrestricted in 3D space, the movement path is largely planar throughout the whole motion. Torsion values were shown to be small from the initial movement phase almost up to the target position. These findings prove that the plane of motion for the whole movement is chosen right from the beginning. Systematic investigations of different obstacle locations and heights confirmed that movement planes reflect obstacle properties. Thus,

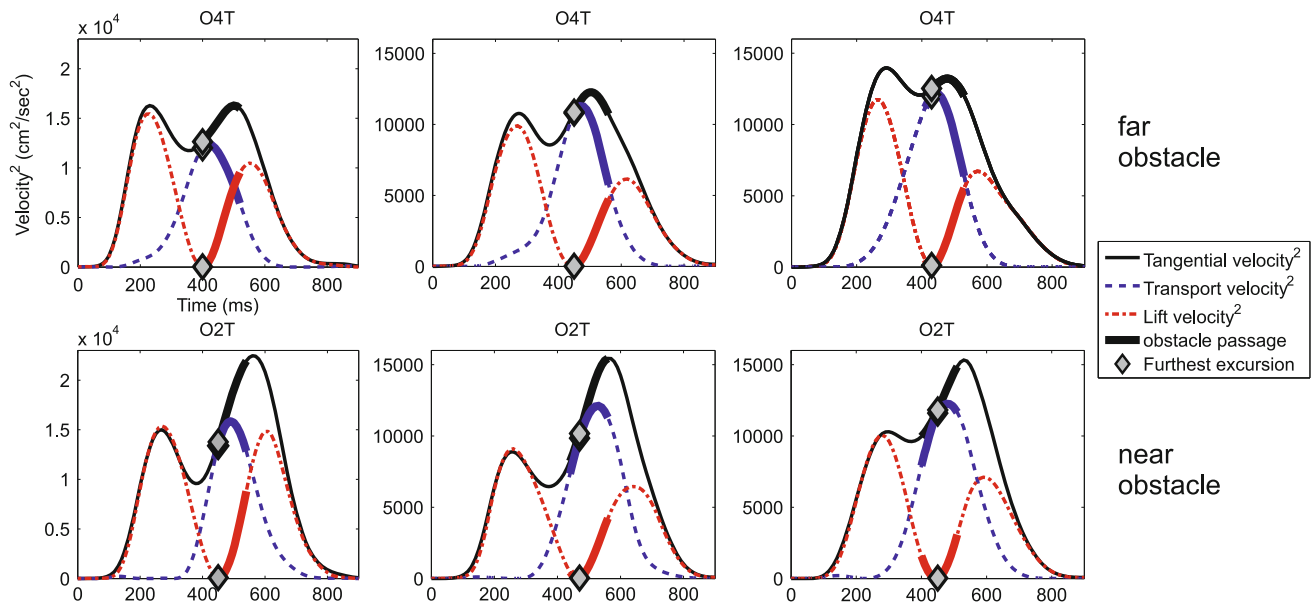


Fig. 12 Single trial velocity for three participants. Obstacle passage and the point of furthest excursion are marked in the velocity profile. For each participant velocities are shown from a movement with a tall

obstacle on the *right* for near obstacles (*beyond*) and for far obstacles (*above*). *Bold lines* denote obstacle passage while *diamonds* indicate the points of furthest excursion

obstacle avoidance affects the motion plan as a whole, not only in the vicinity of the obstacle. Obstacles on the right are usually avoided by going over, and corresponding movement planes are close to vertical. Similarly, obstacles on the left promote a sideways avoidance strategy with a near horizontal plane. Finally, obstacle height also influences the movement plane, whereas lower obstacles are likely avoided over the top (vertical plane), tall obstacles provoke a sideways avoidance (horizontal plane). As both obstacle height and position influence the avoidance strategy, the slope of the resulting plane often represents a combination of both avoidance strategies induced by obstacle configurations.

The global isochrony principle

In Experiment 1, we were able to confirm the validity of the isochrony principle (Viviani and McCollum 1983) according to which movement duration remains approximately constant as travel distance varies. Whereas classical evidence comes from pointing and drawing movements in 2D, we observed isochrony for 3D obstacle avoidance movements. In matching obstacle conditions, avoidance movements to target 1 and target 2 had the same duration, although the traveled distance differed by about 10 %. In light of the observed planarity of the movement paths, the observed isochrony is consistent with the earlier descriptions of that principle (Viviani and McCollum 1983; Viviani and Flash 1995).

Decomposition into lift and transport primitive and structure of velocity

We found that we could decompose the planar trajectory into two movement primitives, the transport primitive and the lift/descend primitive that, to some extent, are independent of each other. The transport component describes the movement from the initial position to the target position along a straight path. The lift and descent sub-movements are the orthogonal complements of the transport component. We were able to show that these components vary independently as obstacle conditions are changed. Shifting the obstacle along the line that links start and target location does not change the lift/descend component while the transport component is initially delayed for obstacles close to the start position. Since we found the lift component to be invariantly bell-shaped, the combined trajectory's shape is largely determined by the transport component. As transport initially stagnates for near obstacle conditions, the lift component dominates the combined trajectory at onset. Symmetrically, the lift component dominates the end of the combined trajectories for far obstacle conditions. This results in overall skewed movement paths (Fig. 9b).

We obtained similar results with respect to obstacle height. While the bell-shaped lift/descend-component scales with obstacle height, the transport component varies little. In the transport component, we did observe, however, an interaction between obstacle proximity and height. The

taller a near obstacle, the more strongly it repels the transport component leading to a slowdown or even to a backward movement. Similarly, far and tall obstacles lead to overshooting the target and to a compensatory reverse movement.

The decomposition into lift/descent and transport components helps to understand the generation and modulation of the double peak structure of tangential velocity. In control conditions without any obstacle, we observe bell-shaped tangential velocities to which the transport primitive provides the main contribution. In most obstacle conditions, tangential velocity has a double peak structure, especially in conditions with tall obstacles in the right part of the workspace that cause avoidance movements with pronounced lift components. Whereas the bimodal lift component provides the main contribution to the first peak, the formation of the second peak is a mixture of both primitives, the transport primitive being predominant in most cases.

Another kinematic observation that can be explained by decomposing the trajectory into primitives is the time structure of acceleration. For all obstacle conditions, the first peak of acceleration occurs at the same time (Fig. 11). This first peak comes largely from the invariant lift component. The acceleration of the transport primitive is often bi-phasic. The first peak of transport acceleration contributes to the first peak in total acceleration. The second peak of transport acceleration provides the main part of the second peak in total acceleration.

The signatures of the lift/descent and transport components are analogous to observations made by Flash and Henis (1991) for 2D aimed arm movements in which the target was abruptly displaced. The authors accounted for the corrected movement as a vector sum of the two trajectory plans (or primitives): the movement from the starting position to the original target position and the movement from the original target position to the shifted target position. They concluded that the initial movement plan was not adapted or modified in response to the target shift but that instead a new plan was added to the previous plan. If we consider the original movement to correspond to the transport component, and the new movement to the lift component, then this observation matches the kind of invariance we have seen, in which one component alone accommodates the required change.

Overduin et al. (2008) and d'Avella et al. (2006) explained reaching movements in primates and humans as the superposition of a small set of muscle synergies, which are scaled and coordinated. They found a reach and a transport related muscle synergy and observed that the synergies were scaled spatially and temporally depending on object size and/or shape (Overduin et al. 2008). In a 2D obstacle avoidance task, Jaric and Latash (1998) found

regularities in joint kinematics that emerged with practice. They interpreted these regularities as synergies: the first, elbow-shoulder synergy being used to move from the initial position to the obstacle, and the second, wrist synergy to move around the obstacle.

Mussa-Ivaldi and Bizzi (2000) proposed that the CNS uses such building blocks to generate a complex and well-timed movement instead of continuously computing an inverse model of the desired trajectory. Our observations could be viewed in that theoretical perspective. The transport and lift component would be two primitives that are scaled according to the target and obstacle configuration. Both components contain parameters that enable the components to adapt to the task conditions, by choosing the direction to the target for the transport component and the plane and elevation of the lift component with respect to the obstacle.

Principles of local and continuous isochrony

In the second experiment, we found that the double peak structure of tangential velocity depended on the distance of the obstacle from the starting position. Near obstacles suppressed the first peak and strengthened the second peak, far obstacles had the reverse effect. These findings are consistent with observations of Flash and Hogan (1985) who investigated 2D movements with predetermined via points. This data can be compared to ours if via points are mapped onto the points of furthest excursion during obstacle passage. The authors observed double peak velocity curves and a modulation of peaks by via points. Whenever a via point was shifted toward either the start or the target position, the velocity peak on the corresponding portion of the movement was higher (Flash and Hogan 1985). The two portions of movement from the start to the via point and from the via point to the target were accomplished within equal movement times. Viviani and Flash (1995) called this effect “local isochrony” but also pointed out that the interplay between global and local isochrony was complex and not fully understood.

Our decomposition of the trajectory into the lift and the transport component throws new light onto local isochrony (see Fig. 13). As the transport trajectory is delayed for near obstacles, transport velocity is initially smaller leading to a low first peak in tangential velocity. The second peak is strengthened because transport velocity compensates toward the end of the movement. In contrast, for far obstacles, a higher first peak in tangential velocity reflects a faster initial transport component (Fig. 13a). Because the lift component has invariant time structure and equal peak velocities for near and far obstacles, the transport component is solely responsible for the local isochrony effect in which the point of furthest excursion is reached at

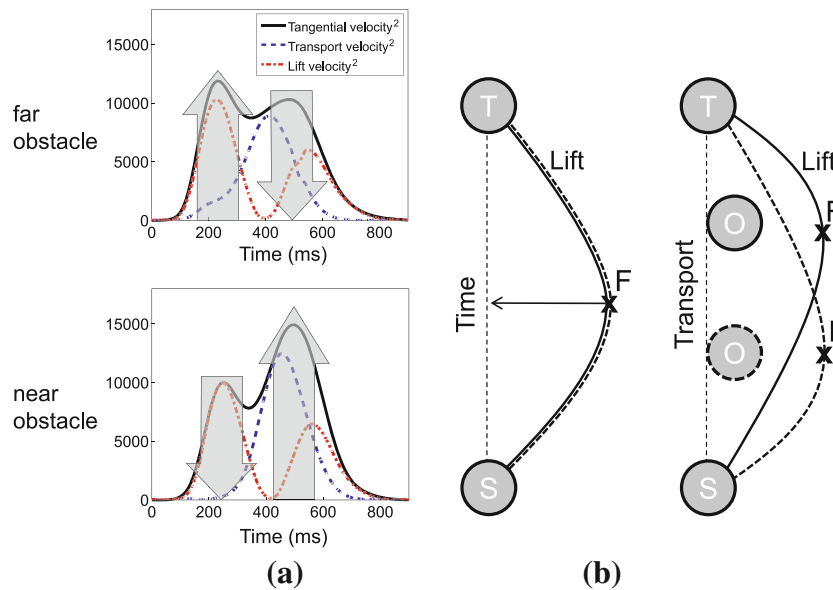


Fig. 13 **a** The modulation of the double peak structure of velocity is achieved by a postponement of the transport primitive for near obstacles, leading to a smaller first peak and a larger second peak in tangential velocity. For far obstacles, a stronger first peak in tangential velocity leads to a higher pace toward the point of furthest excursion (F), enabling an isochronous arriving at this point in near

and far obstacle conditions. **b** The principle of local isochrony is a direct consequence of a constant, *bell-shaped* lift primitive for both obstacle locations. The point of furthest excursion (F) is merely shifted in space, not in time, as the transport component adjusts to obstacle distance

approximately the same time for near and far obstacles. A possible generalization is *continuous isochrony*, according to which the time it takes to reach any percentage excursion (any percentage of maximal lift) is the same for near and far obstacles or via points. The principle of local isochrony is then the special case when looking at the maximum of lift (Fig. 13b).

In this account, there is no direct association between global and local isochrony as the mechanisms from which these principles emerge are different. Whereas global isochrony is achieved by adjusting both the lift and the transport component, local (and continuous) isochrony is the consequence of a constant lift component that forces the transport component to adapt in order to achieve obstacle avoidance.

Time structure of obstacle passage

One might expect a relationship to hold between tangential velocity and the point in time of obstacle passage. Figure 12 showed, however, that passage occurs at different points in the tangential velocity profile for near versus for far obstacles. This is consistent with local isochrony, according to which the point of furthest excursion is coupled to the velocity profile, not the point of obstacle passage. Thus, the tangential velocity profile is not directly correlated to obstacle passage but instead linked to the spatial path. This is consistent with findings of Flash and

Hogan (1985) who reported similarities in the kinematic characteristics of obstacle avoidance movements, unconstrained movement, curved movements, and movements through intermediate targets.

Conclusion

Our investigations show that naturalistic 3D obstacle avoidance movements are surprisingly regular. Most importantly, their kinematic structure can be understood in terms of independent and invariant movement primitives: lift/descent and transport. With this decomposition of movements, we found that relatively complex characteristics of movements like the double peak structure of velocity and the principle of local isochrony can be understood.

Acknowledgments The authors acknowledge support from the German Federal Ministry of Education and Research within the National Network Computational Neuroscience—Bernstein Fokus: “Learning behavioral models: from human experiment to technical assistance”, Grant FKZ 01GQ0951.

References

- Abend W, Bizzi E, Morasso P (1982) Human arm trajectory formation. *Brain* 105(Pt 2):331–348
- Atkeson CG, Hollerbach JM (1985) Kinematic features of unrestrained vertical arm movements. *J Neurosci* 5(9):2318–2330

- Bizzzi E, Mussa-Ivaldi FA, Giszter S (1991) Computations underlying the execution of movement: a biological perspective. *Science* 253(5017):287–291
- Chapman CS, Goodale MA (2008) Missing in action: the effect of obstacle position and size on avoidance while reaching. *Exp Brain Res* 191(1):83–97
- d'Avella A, Portone A, Fernandez L, Lacquaniti F (2006) Control of fast-reaching movements by muscle synergy combinations. *J Neurosci* 26(30):7791–7810
- Dean J, Brüwer M (1994) Control of human arm movements in two dimensions: paths and joint control in avoiding simple linear obstacles. *Exp Brain Res* 97(3):497–514
- Degallier S, Righetti L, Gay S, Ijspeert AJ (2011) Toward simple control for complex, autonomous robotic applications: combining discrete and rhythmic motor primitives. *Auton Robots* 31(2–3):155–181
- Flash T, Henis E (1991) Arm trajectory modifications during reaching towards visual targets. *J Cogn Neurosci* 3(3):220–230
- Flash T, Hogan N (1985) The coordination of arm movements: an experimentally confirmed mathematical model. *J Neurosci* 5(7):1688–1703
- Harris CM, Wolpert DM (1998) Signal-dependent noise determines motor planning. *Nature* 394(6695):780–784
- Hasan Z (1986) Optimized movement trajectories and joint stiffness in unperturbed, inertially loaded movements. *Biol Cybern* 53(6):373–382
- Ijspeert A, Nakanishi J, Schaal S (2001) Trajectory formation for imitation with nonlinear dynamical systems. In: *Proceedings of the IEEE/RSJ International Conference on Intelligent Robots and Systems (IROS2001)*, vol 2, pp 752–757
- Jaric S, Latash ML (1998) Learning a motor task involving obstacles by a multi-joint, redundant limb: two synergies within one movement. *J Electromyogr Kinesiol* 8(3):169–176
- Lacquaniti F, Terzuolo C, Viviani P (1983) The law relating the kinematic and figural aspects of drawing movements. *Acta Psychol (Amst)* 54(1–3):115–130
- Maoz U, Berthoz A, Flash T (2009) Complex unconstrained three-dimensional hand movement and constant equi-affine speed. *J Neurophysiol* 101(2):1002–1015
- Morasso P (1981) Spatial control of arm movements. *Exp Brain Res* 42(2):223–227
- Morasso P (1983) Three dimensional arm trajectories. *Biol Cybern* 48(3):187–194
- Mussa-Ivaldi FA, Bizzzi E (2000) Motor learning through the combination of primitives. *Phil Trans R Soc Lond B Biol Sci* 355(1404):1755–1769, doi:10.1098/rstb.2000.0733
- Overduin SA, d'Avella A, Roh J, Bizzzi E (2008) Modulation of muscle synergy recruitment in primate grasping. *J Neurosci* 28(4):880–892
- Pellizzer G, Massey JT, Lurito JT, Georgopoulos AP (1992) Three-dimensional drawings in isometric conditions: planar segmentation of force trajectory. *Exp Brain Res* 92(2):326–337
- Pollick FE, Maoz U, Handzel AA, Giblin PJ, Sapiro G, Flash T (2009) Three-dimensional arm movements at constant equi-affine speed. *Cortex* 45(3):325–339
- Sabes PN, Jordan MI (1997) Obstacle avoidance and a perturbation sensitivity model for motor planning. *J Neurosci* 17(18):7119–7128
- Saling M, Alberts J, Stelmach GE, Bloedel JR (1998) Reach-to-grasp movements during obstacle avoidance. *Exp Brain Res* 118(2):251–258
- Schaal S, Schweighofer N (2005) Computational motor control in humans and robots. *Curr Opin Neurobiol* 15(6):675–682
- Soechting JF, Terzuolo CA (1987) Organization of arm movements in three-dimensional space. *Wrist motion is piecewise planar. Neuroscience* 23(1):53–61
- Sternad D, Schaal S (1999) Segmentation of endpoint trajectories does not imply segmented control. *Exp Brain Res* 124(1):118–136
- Torres E, Andersen R (2006) Space-time separation during obstacle-avoidance learning in monkeys. *J Neurophysiol* 96(5):2613–2632
- Uno Y, Kawato M, Suzuki R (1989) Formation and control of optimal trajectory in human multijoint arm movement. Minimum torque-change model. *Biol Cybern* 61(2):89–101
- Viviani P, Flash T (1995) Minimum-jerk, two-thirds power law, and isochrony: converging approaches to movement planning. *J Exp Psychol Hum Percept Perform* 21(1):32–53
- Viviani P, McCollum G (1983) The relation between linear extent and velocity in drawing movements. *Neuroscience* 10(1):211–218
- Viviani P, Burkhard PR, Chiu SC, Corradi-Dell'Acqua C, Vindras P (2009) Velocity control in parkinson's disease: a quantitative analysis of isochrony in scribbling movements. *Exp Brain Res* 194(2):259–283